Journal of Power Sources 245 (2014) 175–182

Contents lists available at SciVerse ScienceDirect

Journal of Power Sources

journal homepage: www.elsevier.com/locate/jpowsour

Use of galvanostatic charge method as a membrane electrode assembly diagnostic tool in a fuel cell stack

Pucheng Pei*, Huachi Xu, Xia Zeng, Hongshan Zha, Mancun Song

State Key Lab. of Automotive Safety and Energy, Tsinghua University, Beijing 100084, China

HIGHLIGHTS

- A galvanostatic charge method can be used as a MEA diagnostic tool in a fuel cell stack.
- The EAS, double-layer capacitance, and H_2 crossover current can be calculated.
- The cell ohmic resistance also can be obtained by the voltage transient.
- The RH and temperature have great effects on the measurement.
- The suggested measurement conditions are a certain working temperature and 100% RH.

ARTICLE INFO

Article history:
Received 1 April 2013
Received in revised form
15 May 2013
Accepted 31 May 2013
Available online 14 June 2013

Keywords:
Polymer electrolyte membrane fuel cell
Electrochemical active surface area
Double-layer capacitance
Hydrogen crossover current
Cell ohmic resistance

ABSTRACT

To better measure and monitor the membrane electrode assembly (MEA) status in polymer electrolyte membrane fuel cell (PEMFC) stack, a galvanostatic charge method is improved. The electrochemical active surface area (EAS), double-layer capacitance, hydrogen crossover current, and cell ohmic resistance can be measured by this method. In this method, two or more constant currents are applied to the fuel cell stack, and the voltage response between two electrodes of each cell is recorded and analyzed. Tests on a two-cell stack which is supplied with hydrogen in anode and nitrogen in cathode are carried out, and the influences of temperature and relative humidity (RH) on the MEA parameters are investigated. Results show that with an increase of RH, both double-layer capacitance and EAS increase, while hydrogen crossover current and cell ohmic resistance decrease. With an increase of temperature, hydrogen crossover current increases, cell ohmic resistance decreases, and EAS and double-layer capacitance show little change. The galvanostatic charge method shows a convenient way to research cell consistency and MEA lifetime in a fuel cell stack.

1. Introduction

The membrane electrode assembly (MEA) is one of the most important parts of a polymer electrolyte membrane (PEM) fuel cell, and greatly impacts on fuel cell performances. The MEA aging is the main aspect of fuel cell aging, and the MEA inconsistency is the main factor of cell inconsistency in a stack. Main parameters relating to the MEA aging status and the cell consistency include catalyst active surface area, hydrogen crossover rate, cell resistance and double-layer capacitance.

The cell resistance is one of the reasons resulting in cell voltage drop. The resistance values under different conditions are usually disparate because various factors affect the resistance, such as temperature, membrane thickness, humidification and pretreatment [1]. Techniques such as current interruption [2,3], electrochemical impedance spectroscopy (EIS) [2], and polarization curve have been popularly used to measure the cell resistance.

The double-layer capacitance is physically linked to the space charge (formed by H^+ or H_3O^+) appearing on the electrode–electrolyte interface [4], and its value increases with the area of the double-layer [5,6]. It has been found that the double-layer capacitance is one of the influences on the dynamic performance of a fuel cell [7]. In the past, the double-layer capacitance is measured by the electrochemical methods of EIS [5,6] and cyclic voltammetry (CV) [8].

The hydrogen crossover current is often used to examine leakage or monitor the end of the MEA lifetime [9,10]. Even though the hydrogen crossover current keeps a constant value

* Corresponding author.
E-mail address: pchpei@mail.tsinghua.edu.cn (P. Pei).

0378-7753/$ – see front matter © 2013 Elsevier B.V. All rights reserved.
http://dx.doi.org/10.1016/j.jpowsour.2013.05.201

for almost the whole lifetime of the fuel cell, it increases sharply in the end and leads to fuel cell inefficiency [11]. It makes the open circuit voltage decreased [12], and leads to the degradation of the catalyst layer and membrane [13]. Linear sweep voltammetry (LSV) [14,15] is an electrochemical technique of limiting current to measure the crossover current.

The electrochemical active surface area (EAS) of catalyst layer is an important factor that affects the fuel cell output performance [16–19]. The EAS of catalyst is usually measured by CV, and sometimes the CV cycle is used to make fuel cell decay rapidly [8,20,21]. In CV, a scanned potential is applied between anode and cathode, and the current caused by the cyclic oxidation and reduction of the reactants is measured. We then calculate the total charge of the hydrogen adsorption/desorption process, and get EAS of the catalyst layer.

Previous studies proved that the aging of fuel cell was mainly caused by the degradation of the membrane and catalyst. The degradations of membrane and catalyst usually show in the following ways: i) loss, oxidation, and particle agglomeration in the catalyst layer, resulting in a decrease in EAS [22,23]; ii) PEM thinning, resulting in an increase in gas crossover [24]; iii) aging in membrane, resulting in an increase in resistance [25]. The parameters of the MEA can clearly show the MEA status in the PEM fuel cell, but the methods above need multiple equipment and some of them are not suitable for the measurements of the fuel cell stack. It is necessary to develop a convenient method to investigate the parameters of the MEA in a PEM fuel cell stack.

In this paper, a galvanostatic electrochemical method was performed on a two-cell stack, and tests on the stack were carried out to investigate the effects of temperature and RH on the cell ohmic resistance, hydrogen crossover current, double-layer capacitance and catalyst active surface area.

2. Experimental method

2.1. Fuel cell testing system

Fig. 1 shows a schematic diagram of the experimental setup used in this study. The test station monitored and controlled the gas flow rate, temperature and pressure via the mass flow controller, T-type thermocouple and pressure transducer, respectively. A 3-way valve was easily switched between the air and nitrogen gas. The reactant gas came into the system through the humidifier, and relative humidity was decided by the dew-point temperature. In order to measure each cell voltage, the graphite plates were connected to an NI PXI-1033 data acquisition instrument. The circuit current was measured by a Hall current sensor, and the measurement signal was also collected by the NI PXI-1033 data acquisition instrument. An electronic load was used for the performance tests, while a power supply operated at constant current mode was used for the galvanostatic tests.

2.2. Experiment procedure

A two-cell stack with a 160 cm^2 MEA area was used for the tests in this study. Nafion® N112 membranes were obtained from DuPont de Nemours and the cathode platinum loading was 0.3 mg cm^{-2}. The graphite plates were used for both anode and cathode flow fields. The conditions of experiment procedures were showed in Table 1. An air intake system supplied hydrogen and air to the anode and cathode sides, respectively, for the performance tests. The fuel cell performance was measured as a polarization curve (I–V). After the performance tests, the hydrogen and nitrogen purging were performed for 30 min to avoid the negative impact of residual air. After the purging process, the galvanostatic tests were carried out, and the hydrogen and nitrogen were supplied to the anode and cathode,

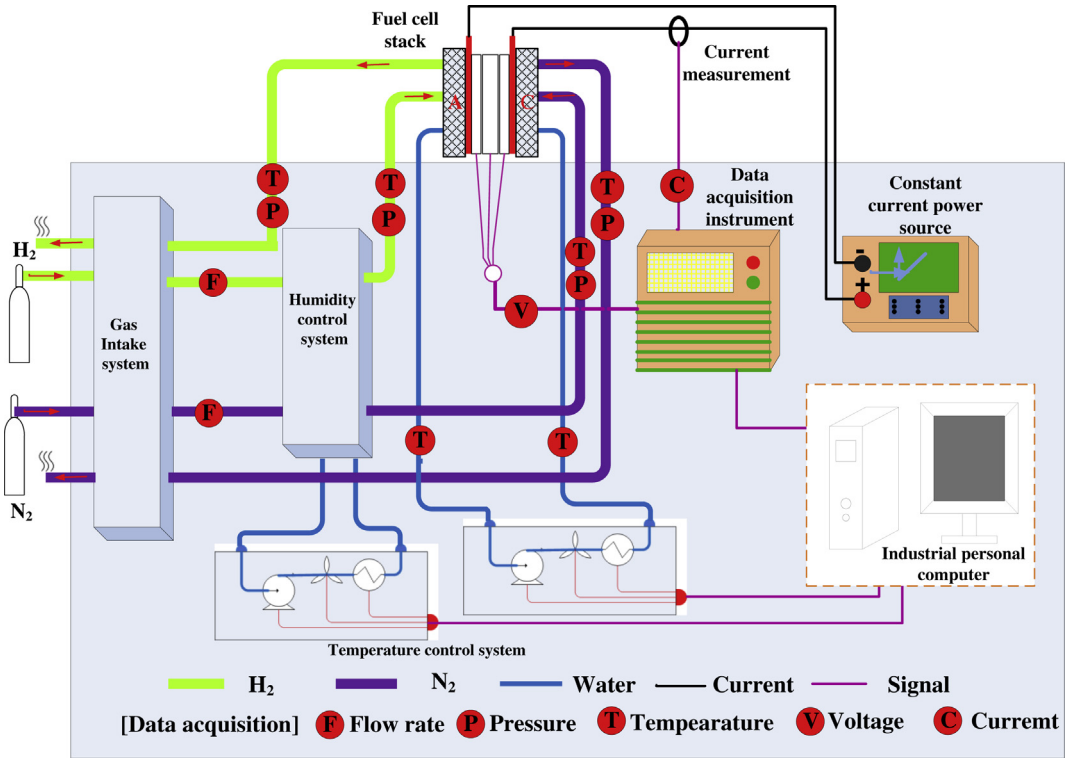

Fig. 1. Schematic diagram of the experimental setup used in this study.

Table 1
Operating conditions for the experiments.

Process No.	Test	Gas supply	Temperature (°C)	RH (%)	Pressure (kPa)	Gas flow
1	Performance tests	A: H_2	45	100	120	Stoichiometric ratios
		C: Air				H_2: 1.5 Air: 2.5
2	Purging process	A: H_2	45	100	120	Flow rates (SLPM)
		C: N_2				H_2: 0.6 N_2: 2
3	Galvanostatic tests	A: H_2	45	100	120	Flow rates (SLPM)
		C: N_2				H_2: 0.6 N_2: 2

respectively, to measure the EAS of the nitrogen side. In the galvanostatic tests, the power supply operated at constant current mode was used to charge the fuel cell stack, resulting in an increase of voltage for each cell. The positive and negative of the power supply were connected to the cathode and anode of the fuel cell stack, respectively. Constant currents of 0.96 A, 1.28 A, 1.60 A, 1.92 A and 2.13 A were supplied during the galvanostatic tests, and when the voltage of each cell reached 0.8 V from the initial voltage, the power source was turned off to avoid damaging the fuel cell [26]. During the charging process, the data acquisition instrument was used for voltage and current signals acquisition.

3. Results and discussion

3.1. Data analysis

A galvanostatic charging method is applied to the fuel cell stack. Fig. 2 shows the voltage changes of two cells under different charging currents in the stack. The voltage data was chopped to show only the hydrogen desorption process. In this figure, the fuel cell shows some similar characteristics with a capacitor. As a sample to obtain the parameters of one MEA in the fuel cell stack, we picked out the data of the No.1 cell in the stack.

3.1.1. H_2 crossover current and double-layer capacitance

The differential charge (dQ) is composed of three parts: i) the charge of the hydrogen desorption (d$Q_{H/Pt}$), ii) the charge of the double-layer being charged (C_{dl}dV), and iii) the charge relating with the hydrogen crossover current (i_{H2}dt), shown as Eqs. (1) and (2), where I_{GA} is the value of a constant charging current, and the double-layer capacitance (C_{dl}) is supposed to be constant, i_{H2} is the hydrogen crossover current.

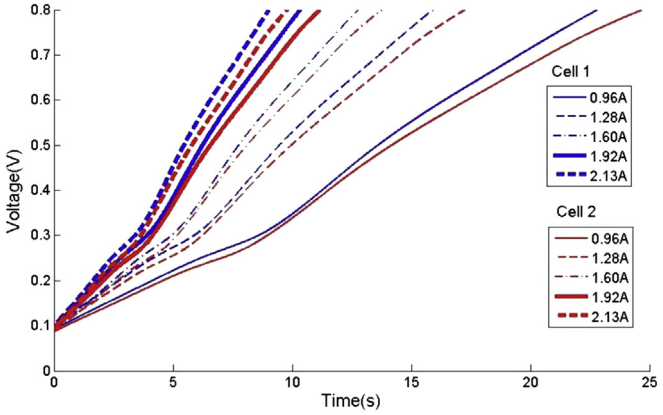

Fig. 2. Voltage curves under various currents in the stack (only the hydrogen desorption process).

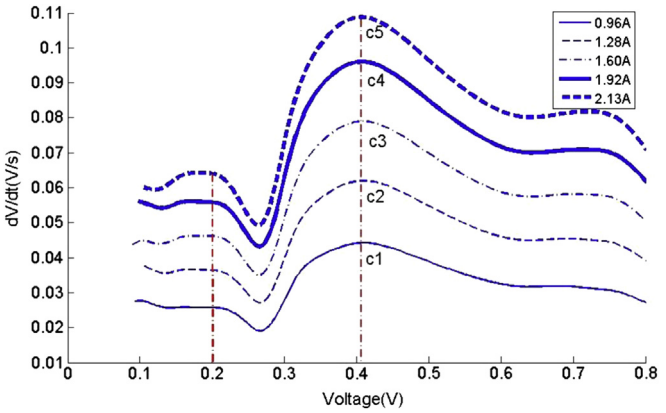

Fig. 3. Voltage change rates under different charging currents.

$$dQ = I_{GA}dt = dQ_{H/Pt} + C_{dl}dV + i_{H_2}dt \quad (1)$$

$$\text{or} \quad I_{GA} = \left(\frac{dQ_{H/Pt}}{dV} + C_{dl}\right)\frac{dV}{dt} + i_{H_2} \quad (2)$$

Fig. 3 shows the voltage change rates under different charging currents. It can be observed that at 0.41 V the voltage change rate gets the maximum value in each curve, meaning the hydrogen desorption process comes to an end ($dQ_{H/Pt}/dV = 0$). At 0.2 V, the voltage change rate in each curve reaches a platform ($dQ_{H/Pt}/dV$ = constant), meaning the hydrogen desorption process is stably performed. Although we do not know the $dQ_{H/Pt}/dV$ value at 0.2 V, we can gain the hydrogen crossover current (i_{H2}) which is the intercept in Fig. 4.

Fig. 4 shows the relationship between charging currents and voltage change rates at 0.2 V and 0.41 V. It can be seen that the intercepts of the two straight lines, which are obtained by the linear fitting method, are almost at the same point, indicating that the hydrogen crossover current keeps a constant value during the charging process, and has no relation with voltage. The hydrogen crossover current density is about 1 mA cm^{-2}. Then, the H_2 crossover rate (J_{H2}) is calculated by Eq. (3), where the faraday constant (F) is 96485 C, A_{MEA} is the MEA effective area. The total capacitance called the MEA capacitance ($C(V)$) can be derived as Eq. (4).

$$J_{H_2} = \frac{i_{H_2}}{2F \cdot A_{MEA}} \quad \left[\text{mols}^{-1}\ \text{cm}^{-2}\right] \quad (3)$$

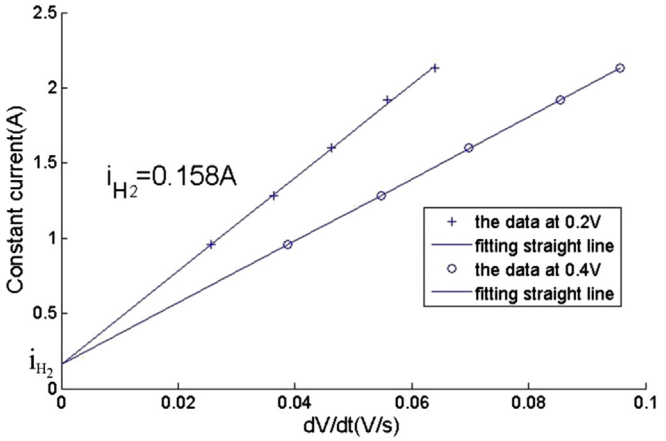

Fig. 4. H_2 crossover current obtained.

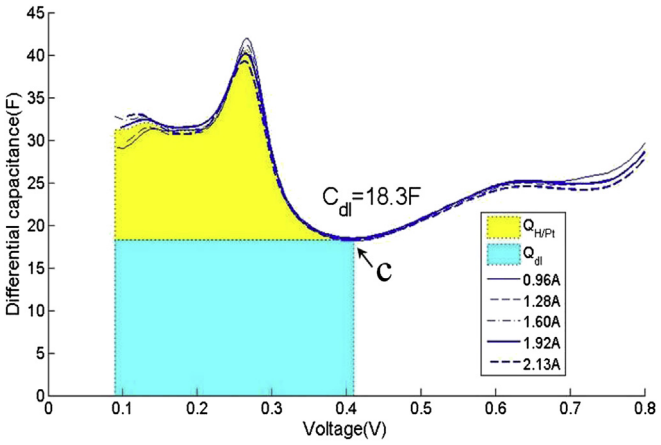

Fig. 5. Curves of MEA capacitance.

$$C(V) = C_{\mathrm{dl}} + \frac{\mathrm{d}Q_{\mathrm{H/Pt}}}{\mathrm{d}V} = \frac{(I_{\mathrm{GA}} - i_{\mathrm{H_2}})\mathrm{d}t}{\mathrm{d}V} \tag{4}$$

After obtaining the i_{H2}, Fig. 5 is draw to show the relationship between MEA capacitance and voltage during charging process for each charging current. According to Eq. (4), it is well known that the minimum value of MEA capacitance (see the point c in Fig. 5) is the double-layer capacitance, where the process of hydrogen desorption ends. The double-layer capacitance of the No.1 cell is 18.3 F. The value shows little difference between the curves of different charging currents in Fig. 5.

According to Eq. (2), when $\mathrm{d}Q_{\mathrm{H/Pt}}/\mathrm{d}t$ is equal to 0, such as the case at 0.41 V in Fig. 3, the C_{dl} and i_{H2} can be also calculated by the Eq. set (5),

$$\begin{cases} I_{\mathrm{GA1}} = C_{\mathrm{dl}}\dfrac{\mathrm{d}V}{\mathrm{d}t}\Big|_{\mathrm{c1}} + i_{\mathrm{H_2}} \\ I_{\mathrm{GA2}} = C_{\mathrm{dl}}\dfrac{\mathrm{d}V}{\mathrm{d}t}\Big|_{\mathrm{c2}} + i_{\mathrm{H_2}} \end{cases} \tag{5}$$

where $\mathrm{d}V/\mathrm{d}t|_{\mathrm{c1}}$ and $\mathrm{d}V/\mathrm{d}t|_{\mathrm{c2}}$ are the voltage change rates (see the point c1 and c2 in Fig. 3), I_{GA1} and I_{GA2} are the charging currents, respectively. The values of C_{dl} and i_{H2} calculated by the Eq. set (5) are shown in Table 2. The results, especially the values of i_{H2}, indicating that the method of linear fitting of multiple points should be more accurate.

3.1.2. Catalyst active surface area

In Fig. 5, the upper part area above the charge of the double-layer capacitance represents the charge of the hydrogen desorption from the catalyst. The desorption charge can be calculated by the curve integral method, shown as Eq. (6), where V_c is the voltage in point c which corresponds to the minimum MEA capacitance.

$$Q_{\mathrm{H/Pt}} = \int_0^{V_c} \left(\frac{I_{\mathrm{GA}} - i_{\mathrm{H_2}}}{\mathrm{d}V/\mathrm{d}t} - C_{\mathrm{dl}} \right) \mathrm{d}V \tag{6}$$

Table 2
The values of C_{dl} and i_{H2} calculated by the Eq. set (5).

Point	$\mathrm{d}V/\mathrm{d}t$	I_{GA}	C_{dl}	i_{H2}
c5	0.09573	2.13	20.54	0.163
c1	0.03878	0.96		
c5	0.09573	2.13	20.72	0.147
c2	0.05470	1.28		
c4	0.08539	1.92	20.60	0.161
c1	0.03878	0.96		

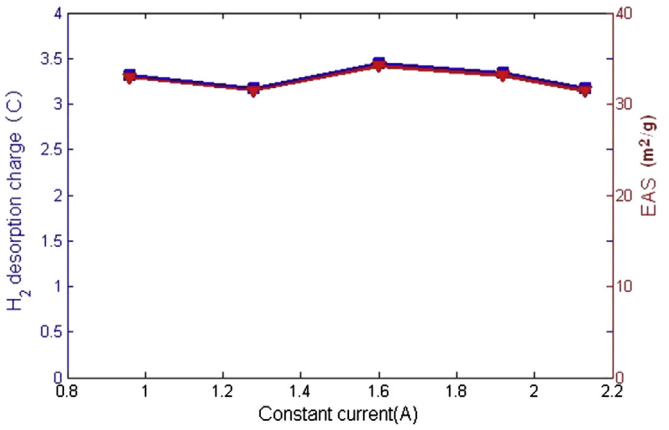

Fig. 6. EAS results of galvanostatic method in this test.

The EAS can be calculated by Eq. (7) [27], where a typical $Q_{\mathrm{H,A}}$ value is 0.21 mC cm^{-2}, W_{Pt} is the platinum loading of the MEA on the cathode side.

$$\mathrm{EAS} = \frac{Q_{\mathrm{H/Pt}}}{Q_{\mathrm{H,A}} \cdot W_{\mathrm{Pt}}} \quad \left[\mathrm{m^2 g^{-1}}\right] \tag{7}$$

The value of W_{Pt}, we know, is often decreasing during the working process of the fuel cell, and it is often unknown for a user. Hence we define the concept of Effective Area Ratio (R_{EA}) as Eq. (8), meaning the ratio between the total electrochemical active surface area and the MEA effective area (A_{MEA}).

$$R_{\mathrm{EA}} = \frac{\mathrm{EAS} \cdot W_{\mathrm{Pt}}}{A_{\mathrm{MEA}}} = \frac{Q_{\mathrm{H/Pt}}}{Q_{\mathrm{H,A}} \cdot A_{\mathrm{MEA}}} \quad [-] \tag{8}$$

Using Eqs. (6)–(8), we achieve Fig. 6 to show the hydrogen desorption charge and the EAS in the No.1 cell for this stack. It shows that the maximum relative error of desorption charge ($Q_{\mathrm{H/Pt}}$) or EAS is no more than 7%. Compared with the CV results [34], the EAS results are much more stable and show more reliability by this galvanostatic method.

3.1.3. Cell ohmic resistance

Fig. 7 shows the whole voltage change process during the constant current charging. A step change in voltage (ΔU) caused by the cell ohmic resistance is observed at the beginning of the curves.

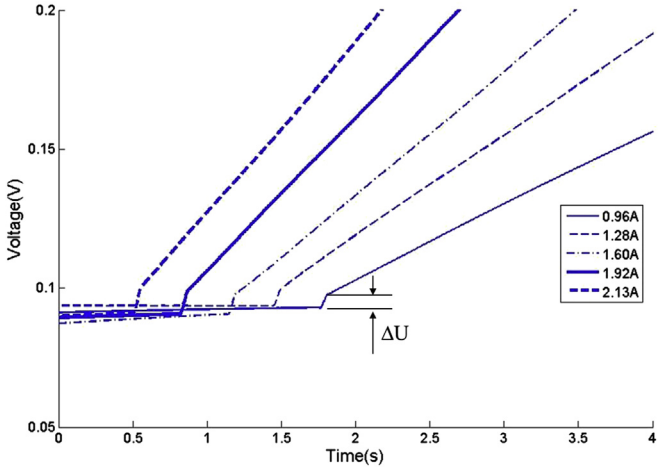

Fig. 7. Voltage transient for the No. 1 cell.

Table 3
The cell resistance of the No.1 cell in the stack.

Temperature (°C)	RH (%)	Cell resistance (Ω cm^2)
45	100	0.79
45	94.5	0.93
45	83.8	1.12
45	61.6	1.44
45	49.8	1.53
50	100	0.72
50	92.3	0.78
50	77.2	0.91
50	69.3	1.29
50	54.6	1.60

This resistance includes the electron resistance throughout the cell and proton resistance in membrane.

The cell ohmic resistance (R_Ω) is calculated by Eq. (9), where ΔU is the step change of the cell voltage. Therefore, the cell ohmic resistance (R_Ω) of the No.1 cell in the stack is shown in Table 3. This method is similar to the method of current interruption [2,3], which is to interrupt the current and to observe the resulting voltage transient. Compared to the current interruption method, the relaxation of electrochemical overpotential in this measurement can be negligible, because of the lack of oxygen reduction reaction.

$$R_\Omega = \frac{\Delta U \cdot A_{MEA}}{I_{GA}} \quad \left[\Omega\ \mathrm{cm}^2\right] \tag{9}$$

The polarization curve of performance tests (process No.1 in Table 1) is shown in Fig. 8. The slope, giving an index to cell ohmic resistance, is 0.918 Ω cm^2, which indicates that the cell ohmic resistance calculated by the above method is reliable. It is worth mentioning that the fuel cell stack, which has been used for research more than 2000 h, is aged, leading to a large cell ohmic resistance.

With the galvanostatic charge method, the MEA status parameters of catalyst active surface area (EAS and R_{EA}), double-layer capacitance (C_{dl}), hydrogen crossover current (i_{H2}), and cell ohmic resistance (R_Ω) can be obtained in a complete measurement, and the status of each MEA in a fuel cell stack can be evaluated.

3.1.4. Analysis of the initial voltage

The cell initial voltage at about 0.1 V is observed before the fuel cell stack is charged, shown in Fig. 7. The initial voltage is also observed in LSV test [15] due to the same gas supply mode of hydrogen and nitrogen. It is caused by a so-called H_2 concentration cell. The hydrogen concentration at the cathode is caused by the hydrogen permeation. The H_2 crossover rate (J_{H2}) is calculated as 2.73 × 10^{-9} mol s^{-1} cm^{-2} by Eq. (3). According to the Nernst equation [28], the theoretical electrode potential of the hydrogen concentration cell (E_{H2}) is calculated by Eq. (10), where R is the gas constant, T is the gas temperature, p'_{H2} is the H_2 partial pressure in cathode, V_m is the mole volume (22.4 L mole^{-1}) and p_{H2}, p_{N2}, Q_{N2} are H_2 pressure in anode, N_2 partial pressure in cathode, N_2 flow rate, respectively, seen in Table 1.

$$E_{H_2} = \frac{RT}{2F}\ln\frac{p_{H_2}}{p'_{H_2}} = \frac{RT}{2F}\ln\frac{p_{H_2}}{p_{N_2}\frac{J_{H_2}A_{MEA}}{Q_{N_2}/V_m}} \tag{10}$$

Therefore, a theoretical electrode potential (E_{H2}) is calculated as 0.102 V, and the value is considered to be consistent with the experimental results, as shown in Fig. 7. The tests of the gas intake mode of H_2/H_2 and N_2/N_2 under the same condition are also performed, and the experimental voltages are both 0 V, proving the existence of the hydrogen concentration cell in a different way.

3.2. Effects of operating conditions on MEA parameters

Tests are carried out applying the galvanostatic charge method to investigate the effects of RH and temperature on MEA status

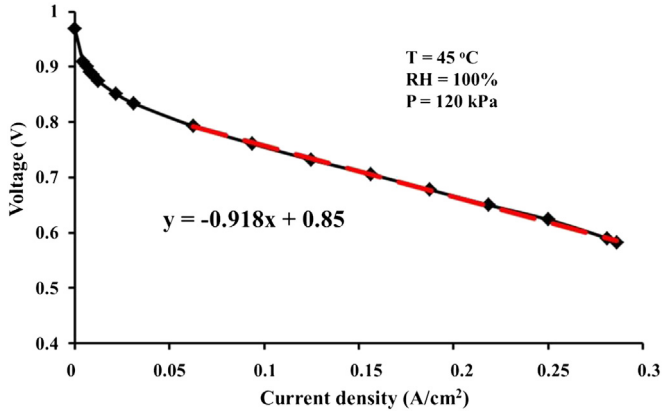

Fig. 8. Polarization curve of No.1 cell in the stack.

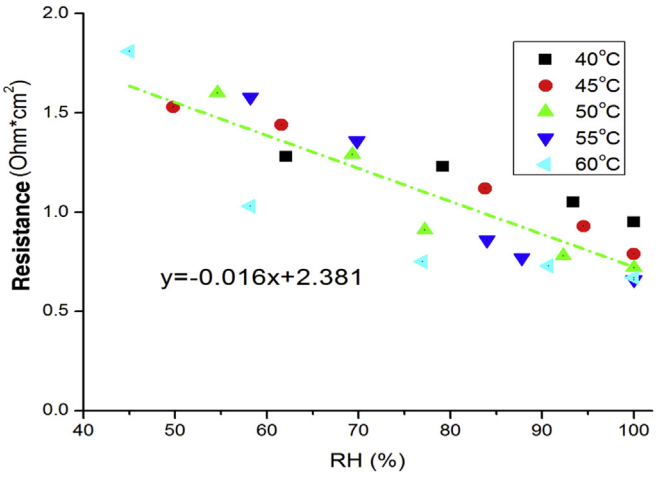

Fig. 9. Cell resistance vs. RH.

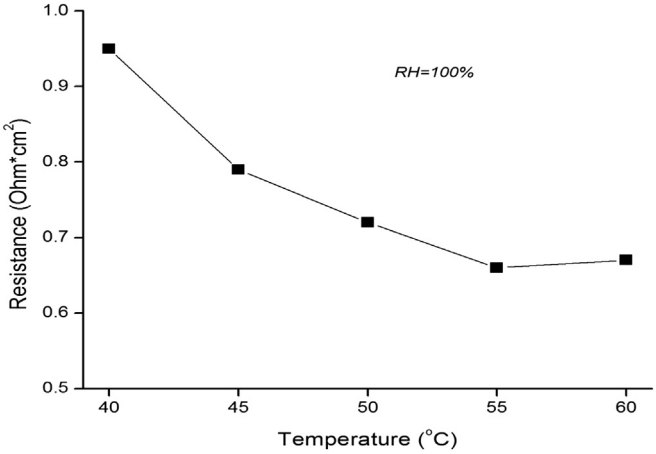

Fig. 10. Cell resistance vs. temperature.

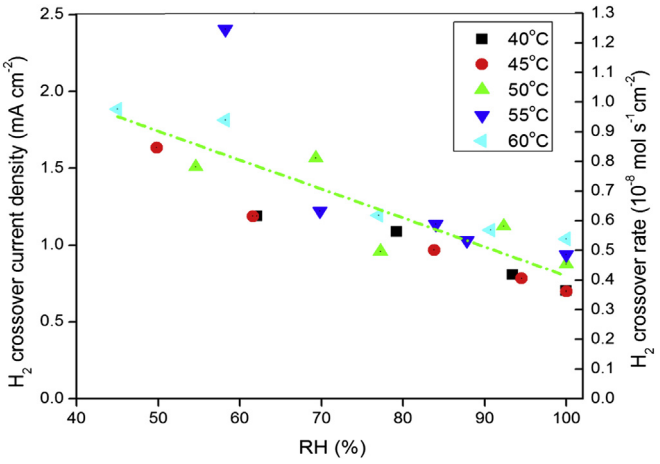

Fig. 11. Hydrogen crossover current vs. RH.

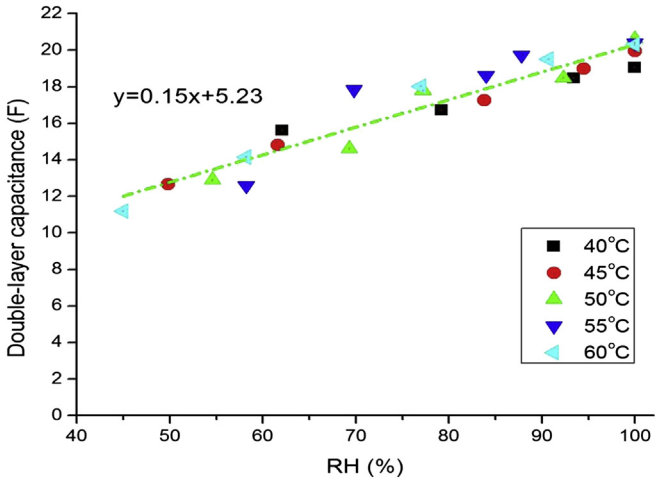

Fig. 13. Double-layer capacitance vs. RH.

parameters. The data of the No.1 cell in the stack above was analyzed to explain the change trends of the parameters.

3.2.1. Cell ohmic resistance

Fig. 9 shows the relationship between cell ohmic resistance and RH at constant temperature. With an increase of RH, the cell ohmic resistance tends to decrease linearly. In the region from 40% to 100% RH, the cell ohmic resistance changes from 1.7 Ω cm^2 to 0.7 Ω cm^2. This is the reason why the *I–V* performance of a fuel cell increases when the reaction gas humidity increases. The reason of resistance decrease is because the proton conductivity increases when more ionic channels are filled with water.

Fig. 10 shows the cell ohmic resistance as a function of temperature at 100% RH. It shows that the cell ohmic resistance decreases when the cell temperature rises, because the electro-osmotic drag of protons becomes easier with a rise of the cell temperature. When temperature reaches 55–60 °C, the resistance has almost no change. So, the performance of fuel cell gets better when the temperature rises.

3.2.2. Hydrogen crossover current

The crossover current results from the H_2 gas permeation which is influenced by the factors such as partial pressure, membrane type, membrane thickness and RH of gases etc. Fig. 11 shows the RH affection on the hydrogen crossover current density and crossover rate at constant temperature. The hydrogen crossover current decreases linearly with an increase of RH. Tang et al. [29] observed a similar trend between the RH and crossover current density. The phenomenon is perhaps as a result of the shrinkage of the micro-channels in PEM. With an increase of RH, the volume of impregnated Nafion polymer increases, which leads to a decrease in the porosity of the PEMs and prevents the permeation of hydrogen.

Fig. 12 shows the trend of the hydrogen crossover current density and crossover rate with a rise of the cell temperature in fully humidified gases. With a rise of the cell temperature, the crossover current density increases linearly. The increase of the hydrogen crossover current may be due to the following factors: (i) when the cell temperature rises, the micro-channels become larger due to expansion, leading to a stronger permeation, and (ii) the molecule movement is also severer at a higher temperature, leading to more hydrogen molecules permeate to the cathode.

3.2.3. Double-layer capacitance

The double-layer capacitance is measured as a function of RH and the results are presented in Fig. 13. It can be seen the capacitance increases with an increase in RH. When RH increases, more area of the platinum surface contacts with water [30], which

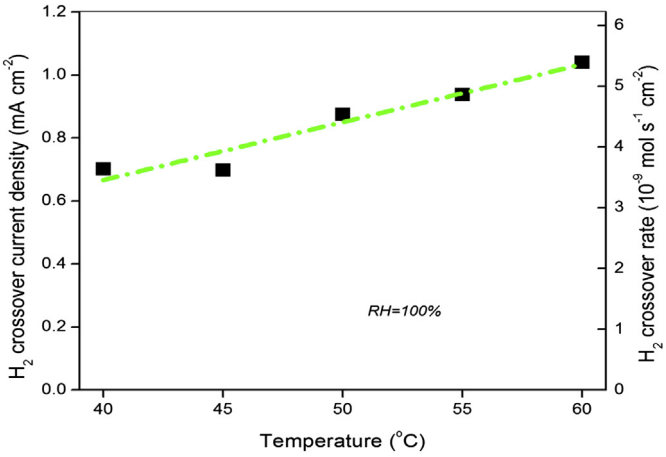

Fig. 12. Hydrogen crossover current vs. temperature.

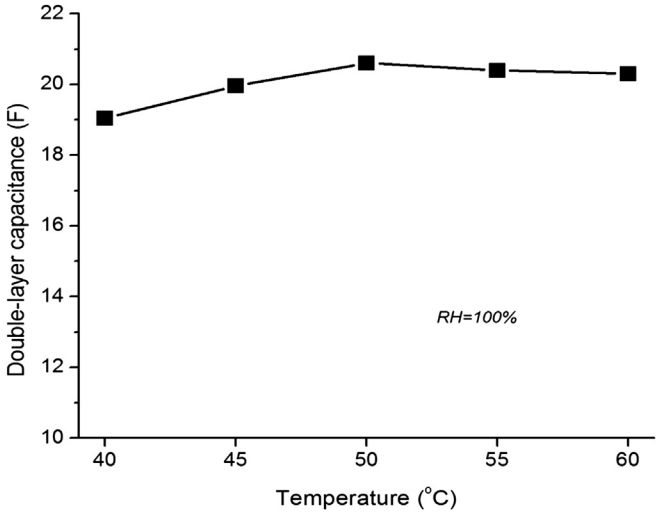

Fig. 14. Double-layer capacitance vs. temperature.

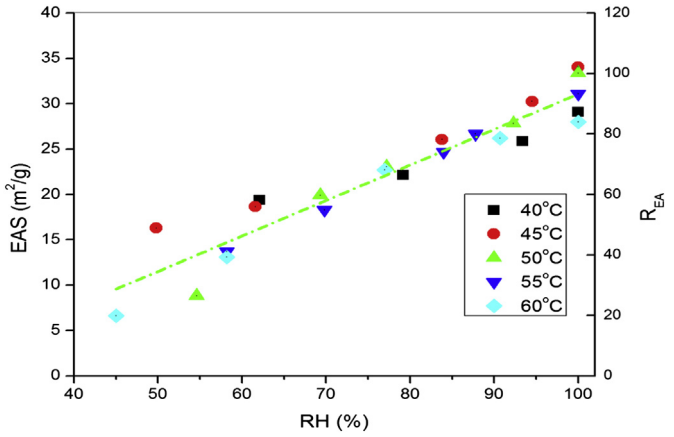

Fig. 15. Catalyst active surface area vs. RH.

attracts more ions. In other words, the area of double-layer forming on the platinum surface becomes larger, resulting in a larger capacitance [5,6]. So, keeping a 100% RH, it is in favor of the fuel cell dynamic loading process.

Fig. 14 shows the trend of the double-layer capacitance with a rise of the cell temperature at 100% RH. The capacitance changes little when the cell temperature rises, which indicates the temperature have less influence on the capacitance. The double-layer capacitance is about 20 F.

3.2.4. Catalyst active surface area

Fig. 15 shows the EAS and R_{EA} as a function of RH at constant temperature. The EAS increases in linear relationship with the RH increase. It is believed that water contributes to the reactions on the surface of Pt. The active sites of the catalyst are the areas that contract water and electrolyte (such as Nafion membrane) [30]. On the other hand, the decrease of water content in catalyst layer prevents some protons access to the platinum surfaces by decreasing the proton channels [31,32]. So, a dry catalyst layers lead platinum to reduce the EAS. In this test, the membrane is humidified by the wet gases. With an increase in gas RH, more water vapor is carried by H_2 and N_2, leading to a large active area and a stronger ability of the proton transfer, which benefits the electrochemical process of the hydrogen desorption on platinum.

Fig. 16 shows the trend of the EAS of platinum with an increase in cell temperature at 100% RH. The EAS decreases when the cell temperature rises from 45 °C to 60 °C, while the EAS increases when the cell temperature rises from 40 °C to 45 °C. Currently there is no clear explanation for the relationship between EAS and temperature. It has been reported that an increase in temperature leads to a decrease in EAS [30]. The cell temperature may affect the water content in catalyst layers, which have a large influence on the active sites of platinum.

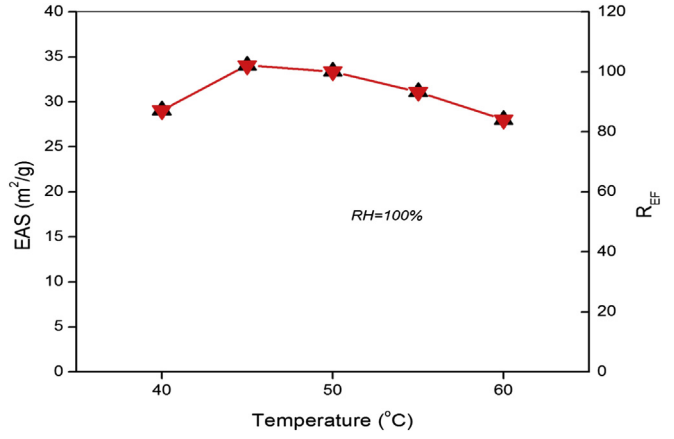

Fig. 16. Catalyst active surface area vs. temperature.

4. Conclusions

A galvanostatic charge method is introduced to evaluate the status of MEA in the PEM fuel cell stack, and the effects of temperature and humidity on the MEA parameters are investigated. It is suggested to perform this method under the condition of a certain working temperature and 100% RH to use this method as an MEA diagnostic tool. Conclusions are drawn as followings:

(1) The galvanostatic charge method can be used to measure catalyst effective area (EAS and R_{EA}), double-layer capacitance, H_2 crossover current, and cell ohmic resistance in stack.
(2) With an increase in RH, the cell ohmic resistance and H_2 crossover current decrease, while the double-layer capacitance and EAS increase. The four parameters of MEA are in linear relationship with RH.
(3) When a rise in temperature, the hydrogen crossover current increases in linear relationship, the cell ohmic resistance decreases, and the double-layer capacitance and catalyst active surface area change little.
(4) The initial voltage is related to the H_2 crossover in galvanostatic test.

Acknowledgments

National Basic Research Program of China (973 Program) (2012CB215505) and 863 Program (2012AA1106012, 2012AA053402), Specialized Research Fund for the Doctoral Program of Higher Education (20090002110074) are gratefully acknowledged for funding this work.

References

[1] D. Brett, S. Atkins, N.P. Brandon, N. Vasileiadis, V. Vesovic, A.R. Kucernak, J. Power Sources 172 (1) (2007) 2–13.
[2] T. Abe, H. Shima, K. Watanabe, Y. Ito, J. Electrochem. Soc. 151 (1) (2004) A101–A105.
[3] T. Mennola, M. Mikkola, M. Noponen, T. Hottinen, P. Lund, J. Power Sources 112 (1) (2002) 261–272.
[4] I. Sadli, M. Urbain, M. Hinaje, J.P. Martin, S. Raël, B. Davat, Energ. Convers. Manage. 51 (12) (2010) 2993–2999.
[5] J. Kim, H. Lee, S. Hong, H.Y. Ha, J. Electrochem. Soc. 152 (12) (2005) A2345–A2351.
[6] Z. Siroma, T. Sasakura, K. Yasuda, M. Azuma, Y. Miyazaki, J. Electroanal. Chem. 546 (0) (2003) 73–78.
[7] M. Eikerling, A.A. Kornyshev, J. Electroanal. Chem. 475 (2) (1999) 107–123.
[8] X. Wang, I. Hsing, P.L. Yue, J. Power Sources 96 (2) (2001) 282–287.
[9] S. Mu, P. Zhao, C. Xu, Y. Gao, M. Pan, Int. J. Hydrogen Energy 35 (15) (2010) 8155–8160.
[10] K. Panha, M. Fowler, X. Yuan, H. Wang, Applied Energy(1) Green Energy; (2) Special Section from papers presented at the 2nd International Energy 2030 Conf., 93, 2012, pp. 90–97.
[11] S.S. Kocha, J. Deliang Yang, J.S. Yi, AICHE J. 52 (5) (2006) 1916–1925.
[12] S.A. Vilekar, R. Datta, J. Power Sources 195 (8) (2010) 2241–2247.
[13] J. Zhang, Y. Tang, C. Song, J. Zhang, H. Wang, J. Power Sources 163 (1) (2006) 532–537.
[14] Y. Song, J.M. Fenton, H.R. Kunz, L.J. Bonville, M.V. Williams, J. Electrochem. Soc. 152 (3) (2005) A539–A544.
[15] V. Ramani, H.R. Kunz, J.M. Fenton, J. Membr. Sci. 232 (1) (2004) 31–44.
[16] N. Cheng, S. Mu, M. Pan, P.P. Edwards, Electrochem. Commun. 11 (8) (2009) 1610–1614.
[17] M.K. Debe, A.K. Schmoeckel, G.D. Vernstrom, R. Atanasoski, J. Power Sources 161 (2) (2006) 1002–1011.
[18] M. Luo, C. Huang, W. Liu, Z. Luo, M. Pan, Int. J. Hydrogen Energy 35 (7) (2010) 2986–2993.
[19] S. Jia, H. Liu, Int. J. Hydrogen Energy 37 (18) (2012) 13674–13680. ICCE-2011.
[20] A. Higier, H. Liu, J. Power Sources 215 (0) (2012) 11–17.
[21] M. Oszcipok, D. Riemann, U. Kronenwett, M. Kreideweis, M. Zedda, J. Power Sources 145 (2) (2005) 407–415.
[22] S. Zhang, X.Z. Yuan, J.N.C. Hin, H. Wang, K.A. Friedrich, M. Schulze, J. Power Sources 194 (2) (2009) 588–600.

[23] S. Mitsushima, S. Kawahara, K. Ota, N. Kamiya, J. Electrochem. Soc. 154 (2) (2007) B153–B158.
[24] V.A. Sethuraman, J.W. Weidner, A.T. Haug, L.V. Protsailo, J. Electrochem. Soc. 155 (2) (2008) B119–B124.
[25] G.B. Jung, K.Y. Chuang, T.C. Jao, C.C. Yeh, C.Y. Lin, Appl. Energy (2012) 81–86.
[26] S. Srinivasan, E.A. Ticianelli, C.R. Derouin, A. Redondo, J. Power Sources 22 (3) (1988) 359–375.
[27] A. Pozio, M. De Francesco, A. Cemmi, F. Cardellini, L. Giorgi, J. Power Sources 105 (1) (2002) 13–19.
[28] N. Kurita, N. Fukatsu, N. Miyamoto, M. Takada, J. Hara, M. Kato, T. Ohashi, Solid State Ionics 162–163 (2003) 135–145.
[29] H. Tang, M. Pan, S.P. Jiang, X. Wang, Y. Ruan, Electrochim. Acta 52 (16) (2007) 5304–5311.
[30] C. Song, Y. Tang, J.L. Zhang, J. Zhang, H. Wang, J. Shen, S. McDermid, J. Li, P. Kozak, Electrochim. Acta 52 (7) (2007) 2552–2561.
[31] J. Zhang, Y. Tang, C. Song, X. Cheng, J. Zhang, H. Wang, Electrochim. Acta 52 (15) (2007) 5095–5101.
[32] H. Kim, K. Song, T.V. Reshetenko, S. Han, T. Kim, S. Cho, M. Min, G. Chai, S. Shin, J. Power Sources 193 (2) (2009) 515–522.